

Dielectronic recombination cross sections for H-like ions

M. S. Pindzola and N. R. Badnell

Department of Physics, Auburn University, Auburn, Alabama 36849

D. C. Griffin

Department of Physics, Rollins College, Winter Park, Florida 32789

(Received 29 January 1990)

Dielectronic recombination cross sections for several H-like atomic ions are calculated in an isolated-resonance, distorted-wave approximation. Fine-structure and configuration-interaction effects are examined in detail for the O^{7+} cross section. Hartree-Fock, intermediate-coupled, multiconfiguration dielectronic recombination cross sections for O^{7+} are then compared with the recent experimental measurements obtained with the Test Storage Ring in Heidelberg. The cross-section spectra line up well in energy and the shape of the main resonance structures are comparable. The experimental integrated cross sections differ by up to 20% from theory, but this may be due in part to uncertainties in the electron distribution function.

I. INTRODUCTION

The dielectronic recombination (DR) of H-like atomic ions is an interesting example of three-body Coulomb field dynamics. The example has been well studied since theoretical calculations of both DR rate coefficients¹⁻⁴ and dielectronic satellite spectra⁵⁻⁹ also have important applications in laboratory and astrophysical plasma research. In this paper we carry out a series of theoretical calculations for the DR cross section of O^{7+} to examine the effects of fine structure and configuration interaction. The calculations are motivated by recent high-resolution experimental measurements¹⁰ for the DR cross section of O^{7+} made with the Heidelberg Test Storage Ring (TSR). Further DR cross-section calculations for C^{5+} , Si^{13+} , and S^{15+} are made to guide future experimental efforts.

The remainder of this paper is arranged as follows. In Sec. II we give a brief outline of the theoretical methods. In Sec. III the results of our DR cross sections for several H-like ions are presented, and in the case of O^{7+} , compared with experiment. A brief summary is contained in Sec. IV.

II. THEORY

In the isolated-resonance approximation, the energy-averaged DR cross section for a given initial level i through an intermediate level j is given by

$$\bar{\sigma}(i \rightarrow j) = \frac{2\pi^2}{\Delta\epsilon k^2} \frac{g_j}{2g_i} \frac{A_a(j \rightarrow i) \sum_k A_r(j \rightarrow k)}{\sum_h A_a(j \rightarrow h) + \sum_h A_r(j \rightarrow h)}. \quad (1)$$

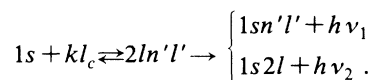
The above equation is in atomic units and $\Delta\epsilon$ is an energy bin width larger than the largest resonance width, k is the linear momentum of the continuum electron, g_j is the statistical weight of the $(N+1)$ -electron doubly excited level, and g_i is the statistical weight of the N -electron target

level. First-order many-body perturbation theory is used to evaluate both the radiative A_r and autoionization A_a rates for the many intermediate levels j in the energy range of interest.

The DR cross section of Eq. (1) is evaluated using two different computational methods. The first method is based on Hartree-Fock wave functions. The atomic structure package of Cowan¹¹ may be used directly to obtain intermediate-coupled configuration-interaction radiative and autoionizing rates from which the DR cross section may be calculated. For doubly excited states involving principal quantum numbers $n > 6$ we made use of the previously written computer code DRFEUD,¹² which calculates intermediate-coupled single configuration DR cross sections for low n explicitly and for high n by extrapolating matrix elements of the dipole radiative and electron-electron Coulomb interactions. The second method is based on Thomas-Fermi-Dirac-Amaldi (TFDA) wave functions. The atomic structure computer code SUPERSTRUCTURE (Ref. 13) developed at University College London was extensively modified to calculate configuration-mixing LS coupling or intermediate-coupling autoionization rates. The resulting computer code AUTOSTRUCTURE (Refs. 14 and 15) calculates LS or intermediate-coupled multiconfiguration DR cross sections for low n explicitly and for high n by extrapolating radial wave functions using quantum-defect theory.

III. RESULTS

For dielectronic recombination in H-like ions we consider the following reaction pathways:



In Table I we present integrated DR cross sections $\bar{\sigma}(i \rightarrow j)\Delta\epsilon$ for O^{7+} through the $2l2l'$ doubly excited states. In column 2 are Hartree-Fock intermediate-

TABLE I. Integrated dielectronic recombination cross sections ($10^{-20} \text{ cm}^2 \text{ eV}$) for O^{7+} . IC represents intermediate coupling while MC represents multiconfiguration.

<i>LS</i> Term	Hartree-Fock		Experiment
	IC-MC	Z expansion	
$2s^2 1S$	0.268	0.260	0.45
$2s2p \ ^3P$	4.897	4.736	4.30
$2p^2 \ ^3P$	0.138	0.310	0.48
$2p^2 \ ^1D$	5.911	6.026	5.65
$2s2p \ ^1P$	1.810	1.868	0.83
$2p^2 \ ^1S$	0.741	0.747	0.61
Total	13.77	13.95	12.3

coupled multiconfiguration results, in column 3 are the Z expansion results of Vainshtein and Safronova,⁵ and in column 4 are the TSR experimental results.¹⁰ The HF results mix only configurations within $2l2l'$. The theoretical predictions for the total integrated DR cross section agree very well, but the experimental results are about 10% below theory.

In Table II we present integrated DR cross sections $\bar{\sigma}(i \rightarrow j)\Delta\epsilon$ for O^{7+} through the $2ln'l'$ doubly excited states as a function of n' . For the row labeled $n' \geq 7$, the cutoff in n' was taken to be 60, although by 40 most of the cross section has been included. The DRFEUD code was used to generate the Hartree-Fock results of column 2 and Cowan's atomic structure codes were used to generate the Hartree-Fock results of column 3, while the AUTOSTRUCTURE code generated the TFDA results of columns 4–7. The TSR experimental results are found in column 8. By comparing the theoretical results in columns 2–7, one can establish the effects of basis orbital choice, fine structure, and configuration interaction (within a $2ln'l'$ complex). The two intermediate-coupling, single-configuration calculations (columns 2 and 6) show that 15% differences result from a choice of basis orbitals in lowest order. By comparing the two intermediate coupling, multiconfiguration calculations (columns 3 and 7) one sees that the effects of basis orbital choice are significantly reduced by including more configurations. The two TFDA, single configuration calculations (columns 4 and 6) show that roughly a 10% increase in the DR cross section results from the inclusion of the fine-structure effects. The two Hartree-Fock, intermediate-coupling calculations (columns 2 and 3)

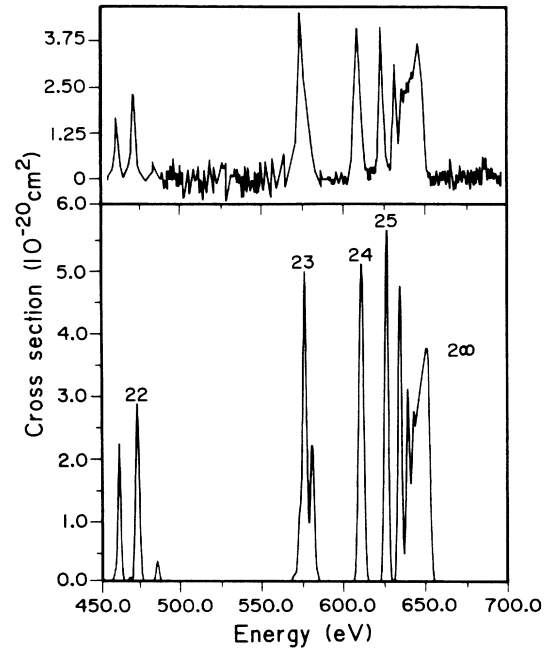


FIG. 1. Dielectronic recombination cross section for O^{7+} . The lower spectrum is from a Hartree-Fock IC-MC cross-section calculation folded with a scaled 2-eV Gaussian energy distribution. The upper spectrum is from the TSR experimental results (Ref. 10).

show that roughly a 15% increase in the DR cross section results from the inclusion of configuration-interaction effects.

The reason for these configuration-interaction and fine-structure effects is that the “weak” autoionization rates get mixed with “strong” autoionization rates and so there is increased access to the dipole radiative channels (see, e.g., Refs. 3 and 15). For example, electrostatic interactions mix the $L=l-1$ term of the $2pnl'l'=l$ and $2pnl'l'=l-2$ configurations; the autoionization rate from the $L=l-1$ term of the “coupled-up” configuration ($l'=l-2$) is much stronger than that from the “coupled-down” ($l'=l$). Also, core fine-structure interactions mix levels of the $2pnl \ ^{1,3}L=l$ *LS*-forbidden autoionizing term with levels of the $2pnl \ ^{1,3}L=l \pm 1$ *LS*-allowed.

TABLE II. Integrated dielectronic recombination cross sections ($10^{-20} \text{ cm}^2 \text{ eV}$) for O^{7+} . *LS* represents *LS* coupling, IC represents intermediate coupling, SC represents single configuration, MC represents multiconfiguration.

	Hartree-Fock IC-SC	Hartree-Fock IC-MC	Thomas-Fermi <i>LS</i> -SC	Thomas-Fermi <i>LS</i> -MC	Thomas-Fermi IC-SC	Thomas-Fermi IC-MC	Experiment
$n=2$		13.8		11.0		11.1	12.4
$n=3$	21.9	23.6	18.2	19.1	18.8	21.7	24.5
$n=4$	16.9	19.1	14.4	16.5	15.1	18.6	18.0
$n=5$	13.0	16.3	10.7	12.7	11.7	15.4	14.3
$n=6$	10.3	13.2	8.1	9.7	9.2	12.0	9.6
$n \geq 7$	46.1		36.2	41.8	39.8	45.1	43.6

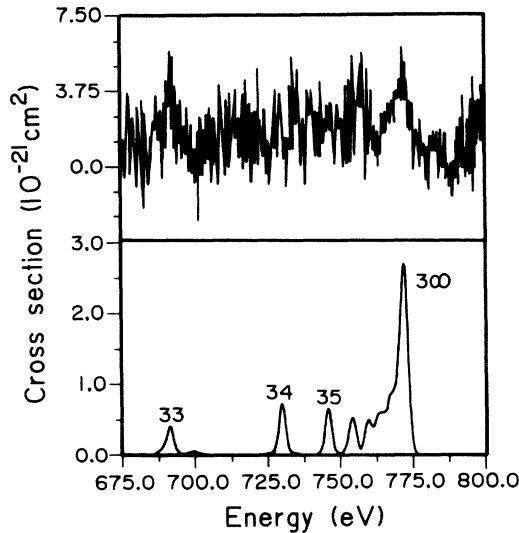


FIG. 2. Dielectronic recombination cross section for O^{7+} . The lower spectrum is from a Thomas-Fermi IC-MC cross-section calculation folded with a scaled 2-eV Gaussian energy distribution. The upper spectrum is from the TSR experimental results (Ref. 10).

If we compare the two intermediate-coupling, multiconfiguration calculations (columns 3 and 7) with experiment (column 8) in Table II, we find that the experimental results differ by no more than 20% from theory. In both Tables I and II the experimental integrated cross sections have been deconvoluted from the observed DR spectrum. Uncertainties in the electron distribution function could account for part of the differences found between theory and experiment. We found that the integrated cross sections for the lower n values were more sensitive to variations in the electron distribution function than those for the higher n values.

In Fig. 1 we compare Hartree-Fock, intermediate-

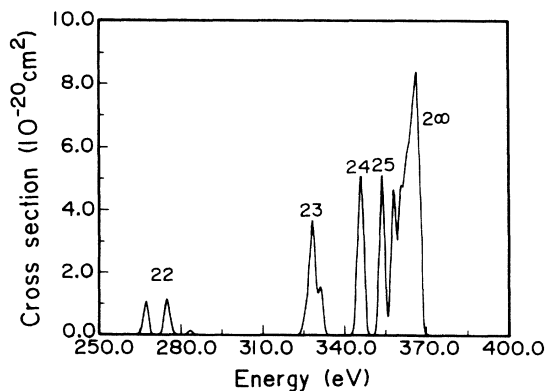


FIG. 3. Dielectronic recombination cross section for C^{5+} . The spectrum is from a Thomas-Fermi IC-MC cross-section calculation folded with a 2-eV Gaussian energy distribution.

TABLE III. Integrated dielectronic recombination cross sections ($10^{-20} \text{ cm}^2 \text{ eV}$) for C^{5+} , O^{7+} , Si^{13+} , and S^{15+} . IC represents intermediate coupling while MC represents multiconfiguration.

	C^{5+}	Thomas-Fermi O^{7+}	IC-MC Si^{13+}	S^{15+}
$n=2$	5.7	11.1	29.1	34.6
$n=3$	14.3	21.7	30.9	30.5
$n=4$	14.0	18.6	20.3	18.4
$n=5$	11.8	15.4	12.6	11.4
$n=6$	10.1	12.0	8.5	7.3
$n \geq 7$	53.4	45.1	25.0	20.5

coupled, multiconfiguration calculations for the DR cross section $\bar{\sigma}(i \rightarrow j)$ for O^{7+} with the TSR experimental results. The theoretical cross section is folded with a Gaussian energy distribution for which a 2-eV width is scaled by a factor of $\sqrt{E/E_0}$, where $E_0=450$ eV, in accordance with best experimental estimates.¹⁰ The peaks in Fig. 1 are labeled as to the nn' values of the intermediate $nl'n'l'$ doubly excited states. Both the theoretical and experimental spectrums line up well in energy and the shape of the resonance structures are quite similar. Caution must be exercised, however, in making a peak to peak comparison between theory and experiment in Fig. 1. We found that both small changes in the energy position of the doubly excited states and small changes in the convolution energy width led to large changes in the height of some of the narrow peaks found in the spectrum of Fig. 1. However, the integrated cross section, which corresponds to the area under the graph, remains unchanged.

In Fig. 2 we compare TFDA, intermediate-coupled, multiconfiguration calculations for the DR cross section $\bar{\sigma}(i \rightarrow j)$ for O^{7+} with the TSR experimental results in the energy region covering the $3ln'l'$ doubly excited states. It appears that background noise in the experiment makes observation of the $3ln'l'$ spectrum difficult,

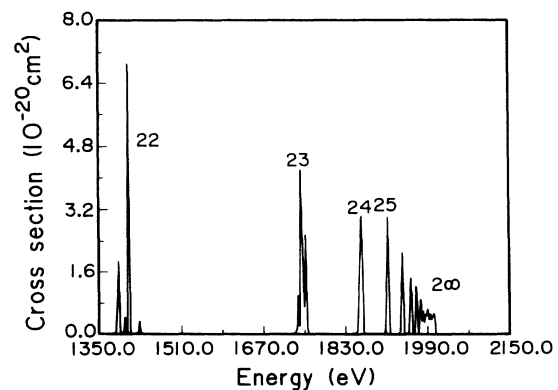


FIG. 4. Dielectronic recombination cross section for Si^{13+} . The spectrum is from a Thomas-Fermi IC-MC cross-section calculation folded with a 2-eV Gaussian energy distribution.

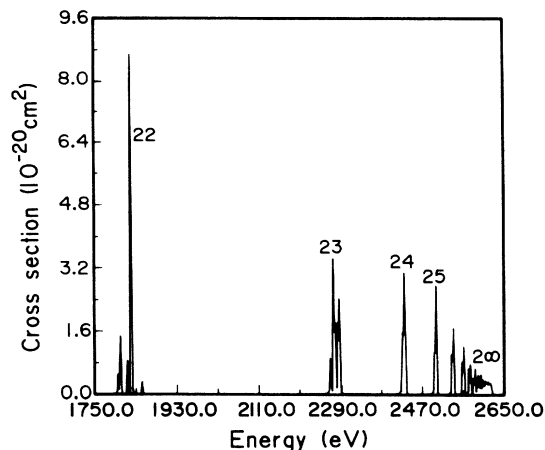


FIG. 5. Dielectronic recombination cross section for S^{15+} . The spectrum is from a Thomas-Fermi IC-MC cross-section calculation folded with a 2-eV Gaussian energy distribution.

except for maybe the 3∞ peak.

To guide future high resolution DR experiments on H-like ions, we present in Table III and Figs. 3–5 further TFDA, intermediate-coupled, multiconfiguration calculations for C^{5+} , Si^{13+} , and S^{15+} . The integrated DR cross sections in Table III provide a convenient test for absolute results, while the 2 eV convoluted DR cross sections in Figs. 3–5 provide an energy positioned spectrum. We include the O^{7+} results in Table III for Z scaling comparison.

The n and Z scaling properties of Coulomb functions are well known (see, e.g., Ref. 16) and can be used to interpret Table III as follows (see also Ref. 17). For a given charge state, A_a scales as n^{-3} , A_r is independent of n , and, excepting the lowest-lying states, k^2 changes little

with n . Thus $\Delta\epsilon\bar{\sigma}$ [see Eq. (1)] scales as n^{-3} for a large enough value of n . For a given value of n , A_r scales as Z^4 , A_a is independent of Z , and k^2 scales as Z^2 . Thus, for low-lying states ($A_r \ll A_a$) $\Delta\epsilon\bar{\sigma}$ scales as Z^2 and for high-lying states ($A_r \gg A_a$) $\Delta\epsilon\bar{\sigma}$ scales as Z^{-2} . For n values such that $A_a \sim A_r$, the Z scaling falls in between the two limits.

IV. SUMMARY

In this paper we carried out a series of dielectronic recombination cross section calculations for several H-like atomic ions. Using different computational methods we probed the sensitivity of the O^{7+} DR cross section to the effect of basis orbital choice, fine structure, and configuration interaction. We then compared the Hartree-Fock, intermediate-coupled, multiconfiguration DR cross sections for O^{7+} with the recent experimental measurements obtained with the TSR in Heidelberg. The DR cross section spectrums line up well in energy and the main resonance structures are similar. The experimental integrated cross sections differ by up to 20% from theory although this may be due in part to uncertainties in the electron distribution function. We look forward to future high-resolution DR measurements at TSR and other heavy ion storage rings providing further stringent tests of many-body calculational methods.

ACKNOWLEDGMENTS

We would like to thank Dr. G. Kilgus, Dr. A. Wolf, and Dr. D. Habs for providing us with the TSR Heidelberg data prior to publication. This work was supported by the office of Fusion Energy, U.S. Department of Energy under Contract No. DE-AC05-84OR21400 with Martin Marietta Energy Systems, Inc. and Contract No. DE-FG05-86ER53217 with Auburn University.

¹A. Burgess and A. S. Tworkowski, *Astrophys. J.* **205**, L105 (1976).

²T. Fujimoto and T. Kato, *Astrophys. J.* **246**, 994 (1981).

³M. Chen, *Phys. Rev. A* **38**, 3280 (1988).

⁴R. Bellantone and Y. Hahn, *Phys. Rev. A* **40**, 6913 (1989).

⁵L. A. Vainshtein and U. I. Safronova, *At. Data Nucl. Data Tables* **21**, 49 (1978).

⁶J. Dubau, A. H. Gabriel, M. Loulergue, L. Steenman-Clark, and S. Volonté, *Mon. Not. R. Astron. Soc.* **195**, 705 (1981).

⁷V. L. Jacobs, J. E. Rogerson, M. H. Chen, and R. D. Cowan, *Phys. Rev. A* **32**, 3382 (1985).

⁸K. R. Karim and C. P. Bhalla, *Phys. Rev. A* **37**, 2599 (1988).

⁹J. Nilsen, *At. Data Nucl. Data Tables* **37**, 191 (1987).

¹⁰G. Kilgus, J. Berger, P. Blatt, M. Griesen, D. Habs, B. Hochadel, E. Jaeschke, D. Krämer, R. Neumann, G. Neurei-

ther, W. Ott, D. Schwalm, M. Steck, R. Stokstad, E. Szmola, A. Wolf, R. Schuch, A. Müller, and M. Wagner, *Phys. Rev. Lett.* **64**, 737 (1990).

¹¹R. D. Cowan, *The Theory of Atomic Structure and Spectra* (University of California, Berkeley, 1981).

¹²D. C. Griffin, M. S. Pindzola, and C. Bottcher, *Phys. Rev. A* **33**, 3124 (1986).

¹³W. Eissner, M. Jones, and H. Nussbaumer, *Comput. Phys. Commun.* **8**, 270 (1974).

¹⁴N. R. Badnell, *J. Phys. B* **19**, 3827 (1986).

¹⁵N. R. Badnell and M. S. Pindzola, *Phys. Rev. A* **39**, 1685 (1989).

¹⁶A. Burgess, D. G. Hummer, and J. A. Tully, *Philos. Trans. R. Soc. London, Ser. A* **266**, 225 (1970).

¹⁷Y. Hahn and K. J. LaGattuta, *Phys. Rep.* **166**, 195 (1988).